RSC Advances

PAPER

View Article Online
View Journal | View Issue

Cite this: *RSC Adv.*, 2019, **9**, 38105

Hot nitric acid diffusion in fluoroelastomer composite and its degradation†

Hailan Kang, *[ab] Long Chen,[a] Hongyang Du,[a] Haoyu Wang,[a] Donghan Li[ab] and Qinghong Fang*[ab]

Received 13th August 2019
Accepted 7th November 2019

DOI: 10.1039/c9ra06286f

rsc.li/rsc-advances

Fluoroelastomers (FKM) are vital sealing materials in acidic environment and their failure can cause severe safety problems. Therefore, investigation of the degradation behavior and mechanism of FKM materials is of great significant. Herein, we investigate a diffusion model of an acidic solution into an FKM composite and its degradation behavior upon immersion in hot nitric acid solution. The results indicate that the diffusion process of the HNO_3 solution into the FKM composite conforms to the Fick diffusion model at a low concentration of nitric acid solution. Besides, the concentration of HNO_3 solution affects the diffusion process of solvent molecules and the dissolution process of the filler particles to some extent. SEM showed that the surface topography of the FKM was significantly altered after it was immersed in HNO_3 solution. The structural and chemical changes of the FKM were studied using ATR-FTIR, SEM-EDS and MAS NMR, which demonstrated the occurrence of decrosslinking *via* hydrolysis of the crosslinks and backbone cleavage by dehydrofluorination. This was also manifested by the decrease in crosslinking degree and mechanical properties. The present study is helpful for revealing the chemical changes in FKM in hot HNO_3 solution.

1. Introduction

Fluoroelastomers (FKM) are key polymers with outstanding properties including high temperature resistance, oil resistance and excellent inertness to solvents, hydrocarbons and acids, which are attributed to the fluorine atoms in their main or side macromolecule chains.[1–6] As desirable materials, FKM are always used as seals, rings, coatings, gaskets, hoses, expansion joints, *etc.* in aircraft, aerospace and vehicle industries. Nowadays, the seals or gaskets made using FKM are usually used as proton exchange membranes for fuel cells and chemical containers, which are subjected to long-term exposure to acidic, alkaline and other chemical solutions.[7–17] Coupled with some factors such as heat and oxygen, chemical solutions can penetrate into sealing materials, causing them to swelling. Once the sealing materials lose their elastic property and seal functionality, the chemical solutions may leak and cause safety problems. Therefore, it is essential to assess and investigate the degradation behavior and mechanism of FKM materials under service conditions to improve their stability and durability.

In the literature, there are many reports on the degradation behavior and mechanism of FKM in various environments. Mitra *et al.*[8,9] focused on the degradation of pure and vulcanized FKM in 10% NaOH solution (an alkaline environment). The results showed that the elimination reaction of fluorine atoms and hydrogen atoms occurred to generated carbon–carbon double bonds, leading to the oxidation of the macromolecules chains and the cleavage of the backbone. Subsequently, Li *et al.*[10,18] demonstrated that the dehydrofluorination of FKM was accompanied with complex oxidation reactions in KOH solution. Wang *et al.*[11] investigated the aging behavior of reactive blends of FKM with polyphenol hydroxyl EPDM in hot air. Akhlaghi *et al.*[12] focused on the degradation of FKM exposed to rapeseed biodiesel at different oxygen concentrations. Xia *et al.*[13] studied the chemical aging behavior of FKM in a simulated proton exchange membrane fuel cell environment, and the influencing factors, including the amount of curing agent, acid-acceptor and filler. Some other reports[19–22] also studied the chemical degradation of other elastomeric materials in a simulated fuel cell solution. However, less attention has been paid to the degradation or corrosion analysis of FKM materials in an acidic environment and the related factors have rarely been investigated.

When elastomeric materials are used as sealing materials in an acidic environment, the diffusion of acidic solutions is regarded as the major influencing factor for their degradation. Acidic solutions can permeate and diffuse into elastomeric materials accompanied by chemical interactions and physical

[a]*College of Materials Science and Engineering, Shenyang University of Chemical Technology, Shenyang, 110142, China. E-mail: kanghailan@syuct.edu.cn; fqh80@126.com*

[b]*Liaoning Provincial Key Laboratory of Rubber & Elastomer, Shenyang University of Chemical Technology, Shenyang, 110142, China*

† Electronic supplementary information (ESI) available. See DOI: 10.1039/c9ra06286f

dissolution processes. The diffusion process of water and other solutions in silicone rubber (SR) has been reported.[23–28] Dai *et al.*[23] indicated that the diffusion of water, NaCl solution, and HNO_3 solution into SR obeys the classical Fick diffusion model. However, Gao *et al.* and Jiang *et al.*[24–26] revealed that the diffusion of water into SR follows the Langmuir diffusion model. Wang *et al.*[27] investigated the absorption characteristics of SR in deionized water, NaCl solution and HNO_3 solution. Unfortunately, the diffusion of acidic solutions into FKM has not been well investigated. The characterization of the diffusion of acidic solution is helpful to further elucidate the degradation mechanism of FKM in acidic environments.

Herein, we focus on the diffusion of hot nitric acid into FKM and the degradation mechanism of FKM in an acidic environment. The weight gain of FKM in hot nitric acid solution was determined *via* a gravimetric method. The physicochemical properties of FKM before and after immersion were investigated *via* Fourier transform infrared spectroscopy (FTIR), nuclear magnetic resonance (NMR), scanning electron microscopy (SEM), swelling tests and mechanical property tests. The diffusion and degradation mechanism of FKM in hot nitric acid solution are discussed and interpreted in detail.

2. Experimental

2.1 Materials

Fluoroelastomer (FKM) was purchased from Zhonghao Chenguang Research Institute of Chemical Industry, which consisted of vinylidene fluoride (VDF, 65–70%), tetrafluoroethylene (TFE, 14–20%) and hexafluoropropylene (HFP, 15–16%). *N*,*N*-Dicinnamylidene-1,6-hexanediamine (crosslinking agent) was supplied by Zigong Hongchuan Chemical Additives Factory. Magnesium oxide (MgO), barium sulfate ($BaSO_4$) and nitric acid (HNO_3) were provided by Tianjin Damao Chemical Reagent Factory. The chemical structure of the fluoroelastomer is shown in the ESI (Fig. S1–S3†).

2.2 Sample preparation

100 g of FKM was compounded with 2 g of crosslinking agent, 20 phr of $BaSO_4$ and 10 phr of MgO as an acid scavenger. The compounds were cured for the optimum curing time (T_{90}) obtained using a vulcameter at 170 °C and then post cured for 12 h at 250 °C.

2.3 Characterization methods

The samples (length × width × thickness, 50 mm × 25 mm × 2 mm) were exposed to different concentrations of HNO_3 solution at 80 °C. The aged sample was taken out and tested at selected times. The weight gain (Q) of the tested sample was calculated using the following equation,

$$Q(\%) = \frac{W_2 - W_1}{W_1} \times 100 \quad (1)$$

where W_1 and W_2 are the weight of the sample before and after the experiment, respectively.

The penetration distance of HNO_3 solution into FKM was observed using an SZTB stereomicroscope (reflected light-oblique illumination, 50 times). The penetration distance of the sample during the immersion process was calculated using the following equation:

$$S = (d_1 - d_2)/2 \quad (2)$$

where d_1 and d_2 are the thickness of the sample before and after the experiment, respectively.

The morphology of the samples was observed using a Model SU8010 SEM system (Hitachi Co., Ltd., Japan) coupled with an energy-dispersive X-ray (EDX) spectrometer. The samples were fractured in liquid nitrogen, and then coated with a thin gold layer. Fourier transform infrared spectra (FTIR) were measured on a Thermo Nicolet nexus 470 FTIR. All spectra were obtained at a resolution of 4 cm^{-1} in the range of 600 to 4000 cm^{-1}. Solid-state ^{13}C and ^{19}F nuclear magnetic resonance (NMR) spectra were measured on an Agilent 600M solid nuclear magnetic spectrometer (Agilent, Palo Alto, CA, USA).

The swelling tests were adopted by immersing the samples in ethyl acetate at 40 °C for 48 h. The swelling index (SI) was calculated using the following equation:

$$\mathrm{SI} = \frac{m_2}{m_1} \quad (3)$$

where m_1 and m_2 are the weight of the sample before and after swelling, respectively.

Tensile tests were performed with dumbbell-shaped samples according to ASTM D412 using an INSTRON 3365 testing machine (Instron Co., USA) with a crosshead speed of 500 mm min^{-1} at room temperature. At least five samples were tested to obtain the average value.

2.4 Analysis method

Fick's second law is applicable to most non-steady state diffusion processes. Fick's second law is as follows:[29]

$$\frac{\partial c}{\partial t} = D\frac{\partial^2 c}{\partial x^2} \quad (4)$$

where c is the concentration of the substance, t is the diffusion time, x is the diffusion distance, and D is the diffusion coefficient.

In the experiment, the weight gain Q_t at time t was obtained from the analytical value corresponding the boundary condition as,[30,31]

$$\frac{Q_t}{Q_\infty} = 1 - \frac{8}{\pi^2}\sum_{n=0}^{\infty}\frac{1}{(2n+1)^2}\exp\left[-\frac{D(2n+1)^2\pi^2 t}{h^2}\right] \quad (5)$$

where t is the time, h is the initial thickness of the sample, and Q_∞ is the equilibrium weight gain of the sample. Since a plot of Q_t *versus* $t^{1/2}$ is linear for a short time, D can be calculated from the initial slope. The equation for short time is

$$\frac{Q_t}{Q_\infty} = \frac{4}{h}\left(\frac{Dt}{\pi}\right)^{1/2} \quad (6)$$

This equation can be rearranged and the diffusion coefficient calculated using the equation:

$$D = \pi\left(\frac{h\theta}{4Q_\infty}\right)^2 \quad (7)$$

where θ is the slope of the initial portion of the plot of Q_t *versus* $t^{1/2}$.

3. Results and discussion

3.1 Weight gain and diffusion process

To reveal the diffusion process of the solution into the materials, the weight gain of the materials was studied. Fig. 1a shows the curves of the weight gain of the FKM composite *versus* the square root of time ($t^{1/2}$) in different concentration nitric acid (HNO_3) solutions at 80 °C. The weight gain of the FKM composite increased with an increase in time and concentration of HNO_3 solution. All the nitric acid solutions diffused freely, resulting in a high weight gain in the composite. When the concentration of the HNO_3 solution was lower than 30 wt%, the weight gain of the FKM composite increased linearly with $t^{1/2}$ in the initial part of the curve, and then reached an equilibrium state. When the concentration of HNO_3 solution was higher than 30 wt%, the weight gain of the FKM composite varied linearly with $t^{1/2}$ throughout the process. As shown in Fig. 1a, the concentration of the HNO_3 solution clearly accelerates the diffusion process. The higher the concentration of the HNO_3 solution, the greater the weight gain of the FKM composite. The weight gain of the FKM composite was over 400% for 50 wt% concentration of HNO_3 solution after 49 days. This large weight gain of the FKM composite is a manifestation of the strong chemical reactions between the acid and the FKM macromolecules, which are not just purely the physical process of diffusion.

The diffusion coefficient is a kinetic parameter that depends on polymer segmental mobility and gives an indication of the rate at which a diffusion process takes place. When the concentration of HNO_3 solution was higher than 30 wt%, the composite could not achieve equilibrium, and thus the diffusion coefficient could not be calculated using eqn (7). The calculated diffusion coefficients (D) are summarized in Table 1, which range from 5.5 to 7.2 $\times$ 10^{-13} m^2 s^{-1}. The diffusion coefficient increased with an increase in the concentration of HNO_3 solution. This behavior is consistent with that postulated in the literature.[23] Fig. 1b shows the theoretical fitting curves according to the Fick model. At a low concentration of HNO_3 solution, it can be seen that Fick's theoretical curve can describe the test results well during the whole absorption process of HNO_3 solution, and it is basically consistent with experimental results. However, at a high concentration of HNO_3 solution, the curves deviate from the shape of the classical Fick curve because of the serious chemical reactions occurring in the diffusion process.

3.2 Penetration distance

The HNO_3 solution entered the interior of the KFM composite from the upper and lower surface areas, thus a permeable layer and non-permeable layer could be clearly distinguished. The diffusion of nitric acid solution in the KFM composite as a function of penetration distance was quantified using a stereomicroscope. The curves of the penetration distance with time are exhibited in Fig. 2. The penetration distance increased rapidly with an increase in the immersion time and concentration of HNO_3 solution, and then slightly increased until achieving a constant value. The penetration distance of the KFM composite ware almost one-half of the thickness of the sample after 25 days, indicating that the HNO_3 solution fully penetrated the FKM composite (Table 2).

3.3 Morphology and EDS analysis

Fig. 3 shows the photographs of the FKM composite after it was immersed in different concentrations of hot HNO_3 solution at 80 °C. The color of the sample changed from brown to reddish brown, and finally orange, while the sample was seriously deformed with an increase in the concentration of the HNO_3 solution. To further investigate the morphology changes in the FKM composite in HNO_3 solution, SEM images were obtained,

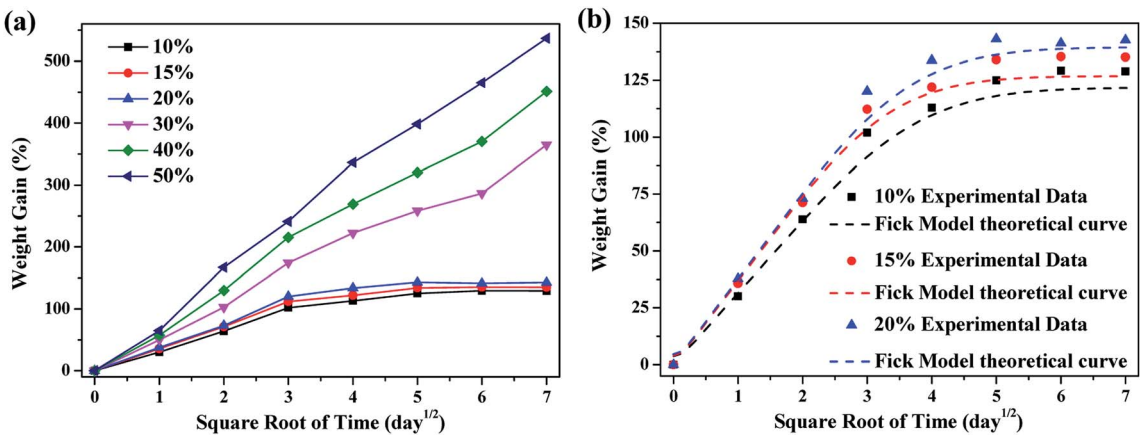

Fig. 1 (a) Relative weight gain and (b) Fick model for the diffusion of different concentrations of HNO_3 solution in the FKM composite.

Table 1 Experimental evaluation of the diffusion parameters for the diffusion of HNO_3 solution into the FKM composite at 80 °C *via* a gravimetric method

Concentration of HNO_3 solution	10%	15%	20%
$D_f \times 10^{13}$ (m^2 s^{-1})	5.50	6.34	7.18

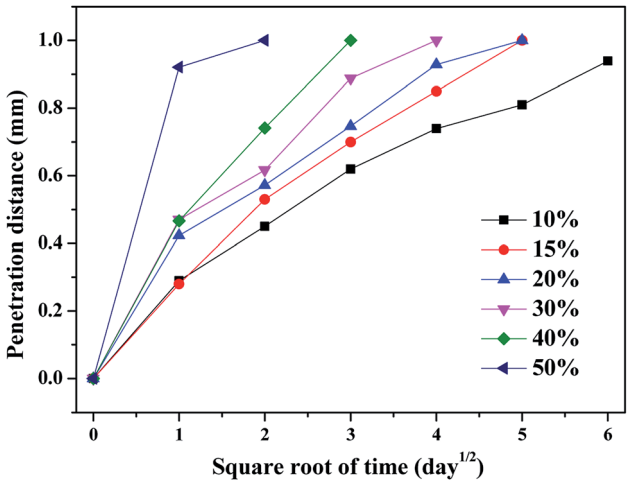

Fig. 2 Penetration distance curves for the diffusion of different concentrations of HNO_3 solution in the FKM composite.

as shown in Fig. 4. The FKM composite without immersion exhibited a relatively smooth surface, whereas the FKM composite after immersion for 36 days showed a very rough and irregular surface with the sporadic presence of small holes. This indicates that some changes in the surface of the composite occurred due to the chemical degradation of FKM in HNO_3 solution, as confirmed by the following discussion on the FTIR results.

The EDS results prove that the surface of the FKM composite contains 7 major elements, which are C, F, O, N, Mg, Ba and S, and these elements imply the existence of $BaSO_4$ and MgO. For the FKM composite after immersion in HNO_3 solution, the content of C dramatically increased and the content of F obviously decreased compared with that of the FKM composite without immersion, indicating that the elimination of hydrogen fluoride (HF) occurs through dehydrofluorination induced by the harsh acidic environment. Additionally, the contents of Mg, Ba and S clearly declined, manifesting that these elements as ions dissolved in the HNO_3 solution.

3.4 ATR-FTIR

To further analyze the chemical degradation phenomena of the FKM composite exposed to HNO_3 solution, FTIR spectroscopy was performed. Fig. 5 shows the FTIR spectra of the FKM composite immersed in HNO_3 solution for different times. For the FKM composite without immersion, the peaks at ~1398 cm^{-1}, ~1164 cm^{-1} and ~889 cm^{-1} are assigned to the stretching vibrations of $-CF_3-$, $-CF_2-$ and –CF–, respectively. The peak at ~1648 cm^{-1} is assigned to the C=C stretching vibration because the dehydrofluorination of FKM by the base generates doubles bonds in the backbone chain during the vulcanization procedure.[9] The peak located at ~1079 cm^{-1} is attributed to the stretching vibration of C=N, demonstrating a crosslinking reaction occurred for the FKM. For the FKM composite immersed in HNO_3 solution, an increase in intensity for the peak located at ~1648 cm^{-1} was observed, which is due to the elimination of hydrogen and fluoride atoms, namely the dehydrofluorination reactions. Because C=C is easily attacked by aqueous acid to generate –OH, a new peak at 3382 cm^{-1} attributed to the stretching vibration of O–H emerged and became stronger as a function of immersion time. Besides, the stretching vibration of C=N gradually became weaker as a function of immersion time because of the hydrolysis of the crosslinks accompanied with the introduction of –OH groups. Moreover, Fig. 5b presents the percentage change in A_{CF}/A_{CF_3} (the ratio of the FTIR absorbance of CF to CF_3) and A_{CF_2}/A_{CF_3} (the ratio of the FTIR absorbance of CF_2 to CF_3) as a function of immersion time, where the absorbance of CF_3 is non-reactive and used as a reference. The curves show that the percentage change in A_{CF}/A_{CF_3} and A_{CF_2}/A_{CF_3} decreased with an increase in immersion time. This decrease in fluorine content is attributed

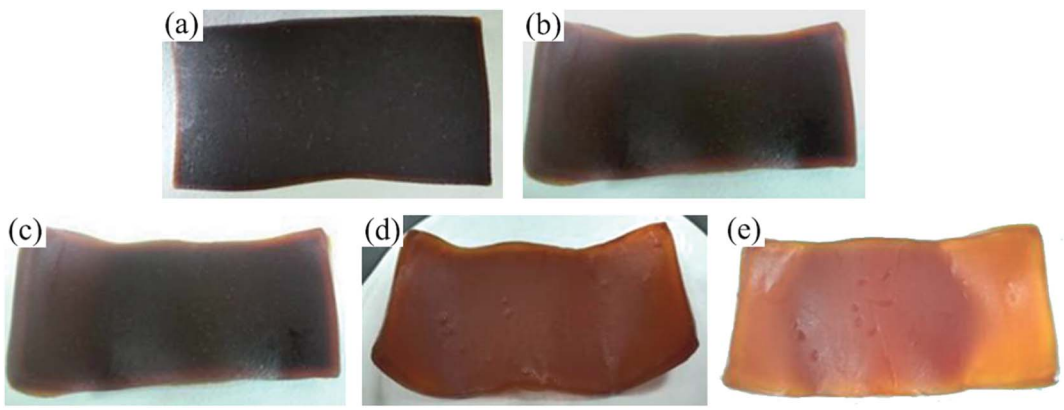

Fig. 3 Photographs of the FKM composite immersed in different concentrations of HNO_3 solution after 36 days: (a) 10 wt%, (b) 20 wt%, (c) 30 wt%, (d) 40 wt%, and (e) 50 wt%.

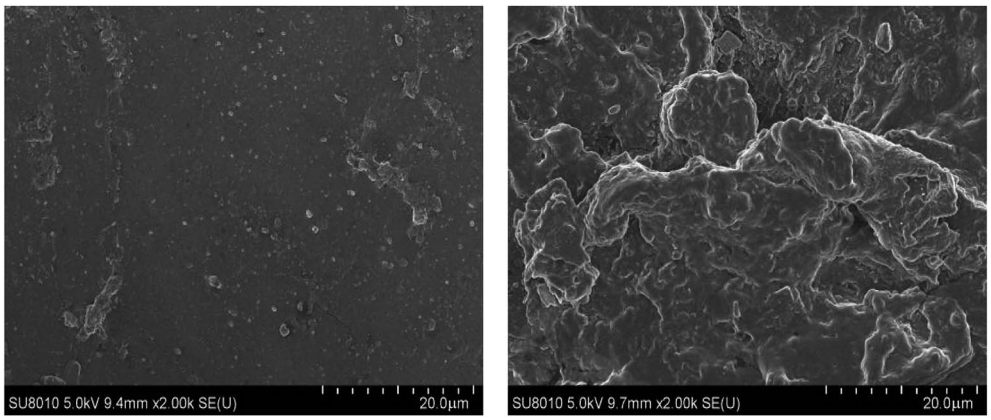

Fig. 4 SEM images of the FKM composite (left) before (right) after immersion for 36 days in 50 wt% HNO_3 solution.

Table 2 EDS data of FKM composite (a) before (b) after immersion for 36 days in different concentrations HNO_3 solution at 80 °C

	10 wt%		30 wt%		50 wt%	
Concentration of HNO_3 solution	(a)	(b)	(a)	(b)	(a)	(b)
F	45.6	32.9	46.8	24.2	45.9	23.4
C	28.2	44.3	26.8	48.4	27.2	36.0
O	10.4	15.7	11.1	20.4	11.3	34.3
N	3.3	5.7	3.8	5.3	3.7	5.0
Mg	5.3	0.6	5.6	0.6	4.0	0.7
Ba	5.3	0.5	4.3	0.7	5.6	0.1
S	1.9	0.3	1.6	0.4	2.3	0.5

to the dehydrofluorination reaction. As shown in Fig. 5b, the peaks at 2917 cm^{-1} and 2849 cm^{-1} are attributed to the anti-symmetric and symmetric stretching vibrations of $–CH_2–$, respectively, which emerge noticeably and simultaneously as a function of immersion time. This indicates an increase in the dominance of methylene over fluorine in the FKM backbone, which is also a manifestation of the degradation process.[12] The ATR-FTIR observations are consistent with the EDS results, demonstrating that significant structural and chemical changes occurred in the FKM backbone and crosslinking point.

The FTIR spectra of the FKM composite immersed in different concentrations of HNO_3 solution are exhibited in Fig. 6. All the curves present similar absorption peaks. However, a significant change is the percentage of A_{CF}/A_{CF_3} and A_{CF_2}/A_{CF_3} (Fig. 6b). The percentage of A_{CF}/A_{CF_3} and A_{CF_2}/A_{CF_3} increased with an increase in the concentration of HNO_3 solution, demonstrating the dehydrofluorination reaction, as discussed earlier.

3.5 MAS-NMR

The solid-state ^{13}C and ^{19}F MAS-NMR spectra of the FKM composite are shown in Fig. 7. As shown, the ^{13}C MAS-NMR spectra of the FKM composite immersed in HNO_3 solution are similar to that of the FKM composite without immersion. The multiplets at 106–117 ppm are assigned to the carbon atom connected with a fluorine atom (C–F). The peak centered at 88 ppm is assigned to the double bonds (C=C), which confirms the occurrence of the dehydrofluorination reaction. The

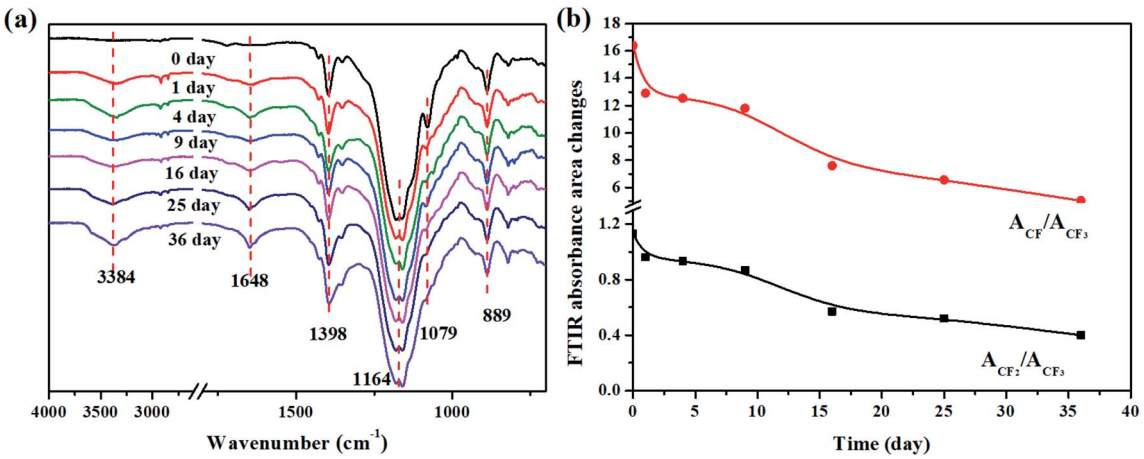

Fig. 5 (a) FTIR spectra and (b) FTIR absorbance area changes in A_{CF}/A_{CF_3} and A_{CF_2}/A_{CF_3} of FKM composite immersed in 20 wt% HNO_3 solution.

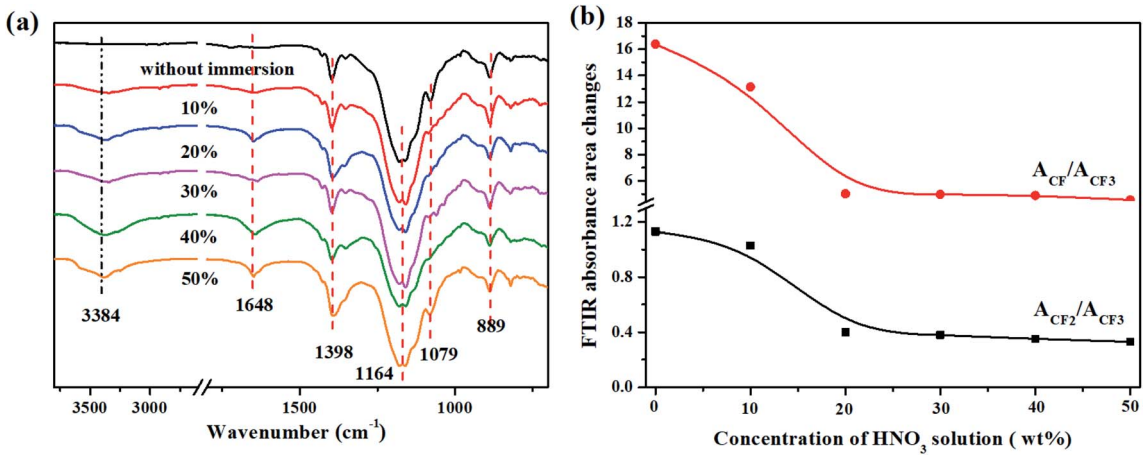

Fig. 6 (a) FTIR spectra and (b) FTIR absorbance area changes in A_{CF}/A_{CF_3} and A_{CF_2}/A_{CF_3} of FKM composite immersed in different concentrations of HNO_3 solution.

multiplets at 33–40 ppm are assigned to the carbon atom connected with a hydrogen atom (C–H). To characterize the chain structures in detail, ^{19}F MAS-NMR was also performed. The peak centered at −58 ppm is assigned to –CF═C(CF_3)–, corresponding to the peak at 88 ppm in the ^{13}C MAS-NMR spectrum; the peak centered at −75 ppm is assigned to the –CF_3 groups from the HFP sequences; the multiplets at −83–165 ppm are assigned to the –CF_2– groups from the HFP, VDF and TFE sequences; and the peak centered at −185 ppm is assigned to the –CF– groups from the HFP sequences. In addition, these peaks all correspond to the peak at 106–117 ppm in ^{13}C MAS-NMR spectrum. As shown in Fig. 7, compared with the ^{13}C and ^{19}F MAS-NMR spectra of the FKM composite without immersion, the peak intensity for the FKM composite immersed in HNO_3 solution was reduced sharply.

Furthermore, the molar fractions (mol%) of –C═C– in the FKM composite was calculated using eqn (8),

$$X_{C=C} = \frac{I_{-58}}{I_{-58} + I_{-75}} \times 100\% \quad (8)$$

The molar fractions of –C═C– in FKM composites were about 2.8 mol% (without immersion), 4.3 mol% (20 wt% HNO_3) and 11 mol% (50 wt% HNO_3). This result indicates that the hot HNO_3 solution diffused into the FKM composite and caused the dehydrofluorination and degradation reaction, as manifested by the ATR-FTIR results.

3.6 Swelling studies

The equilibrium-swelling experiment was employed to characterize the crosslinking degree. Fig. 8 shows the swelling index of the FKM composite after immersion in HNO_3 solution. The swelling index increased as the immersion time and the concentration of the HNO_3 solution increased. A higher equilibrium swelling index corresponds to a lower crosslinking degree. Thus, the increase in the swelling index indicates that decrosslinking is a primary process for the chemical degradation and becomes more evident with an increase in the concentration of HNO_3 solution. In the swelling tests, the samples immersed in a higher concentration of HNO_3 solution

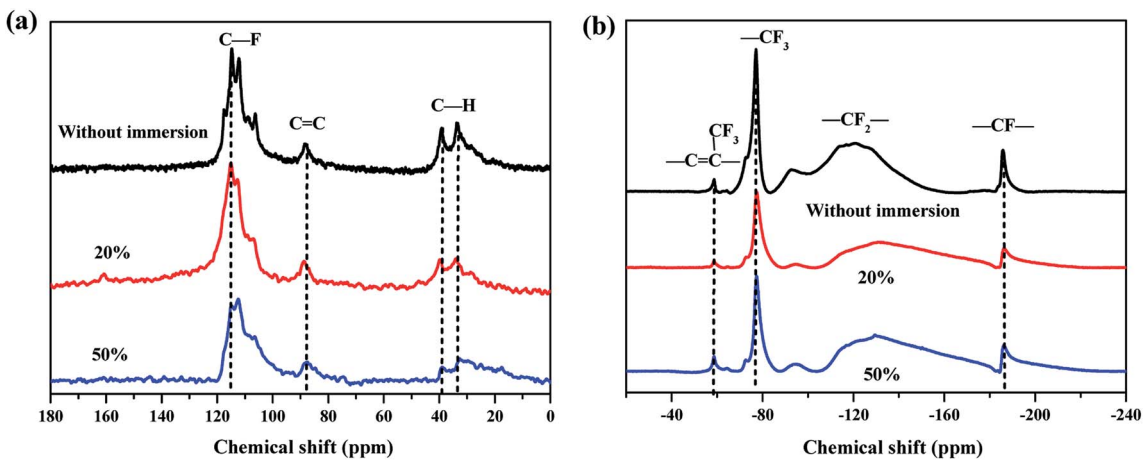

Fig. 7 (a) ^{13}C and (b) ^{19}F MAS-NMR spectra of FKM composite immersed in 20 wt% and 50 wt% HNO_3 solution.

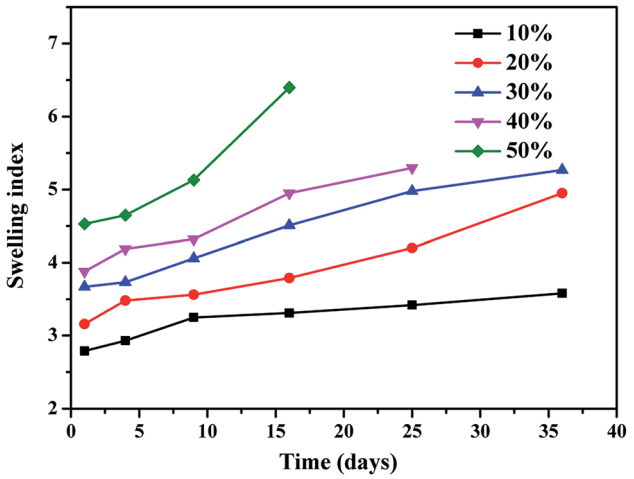

Fig. 8 Swelling index of FKM composite after immersion for 36 days in different concentrations HNO_3 solution.

crumbled into powders, and thus no swelling index was available.

3.7 Mechanical properties

The mechanical properties of elastomeric materials are vital in their failure. Thus, the changes in the mechanical properties of the FKM composite immersed in HNO_3 solution were investigated. Fig. 9 shows the tensile strength and elongation at break of the FKM composite immersed in HNO_3 solution for different times. Tensile strength is a complex function of the nature and type of crosslinks, crosslinking density, chemical structure of the rubber, and changes associated with degradation.[32,33] The FKM composite showed a significant decrease in tensile strength when immersed in the hot HNO_3 solution, and as the concentration of the HNO_3 solution and immersion time increased, the tensile strength of the FKM composite declined more strongly. The tensile strength decreased from 12.0 MPa to 2.4 MPa after 10 days for the FKM composite immersed in 20 wt% HNO_3 solution, and also decreased from 12.0 MPa to 0.8 MPa for the FKM composite immersed in 50 wt% HNO_3 solution. In contrast, the elongation at break of the FKM composite increased with an increase in the concentration of HNO_3 solution and immersion time. Thus, the deterioration in the mechanical properties of the FKM composite is a manifestation of the hydrolysis of its crosslinks, which is consistent with the FTIR results and swelling studies.

3.8 Degradation mechanism

As discussed above, it is clearly indicated that the FKM composite was subjected to a large degree of physical and chemical changes in a hot HNO_3 solution. The physical changes caused a variation in its mass and penetration distance, while the chemical changes were reflected by the destruction of its chemical structure. The plausible diffusion and degradation mechanisms are depicted in Scheme 1, as fully manifested by the above analysis.

The diffusion process can be explained as follows. In the initial stage, the H_2O and HNO_3 molecules can rapidly enter the macromolecular networks owing to the high concentration difference in solvent between the inside and outside of the FKM composite. Moreover, the FKM macromolecule chains decrosslink and break in the acidic solution. Consequently, the macromolecular chains move towards the outside, and generate a larger internal free volume, resulting in more solvent molecules entering and a faster diffusion rate. Besides, the highly elastic FKM possesses a larger free volume in hot acid solution, which is beneficial for the diffusion of HNO_3 solution. In practice, the small molecule additives and fillers in FKM are dissolved in HNO_3 solution, and thus in the later stage, a slow diffusion rate towards swelling equilibrium at long immersion times occurs.

Meanwhile, in the diffusion process, structural and chemical changes in the FKM elastomer occur, including decrosslinking *via* hydrolysis of the crosslinks and backbone cleavage by dehydrofluorination. FKM elastomers cured by diamine are prone to hydrolysis in the presence of hot water.[12,20,21] The degradation of FKM elastomer initiates at the weakest links

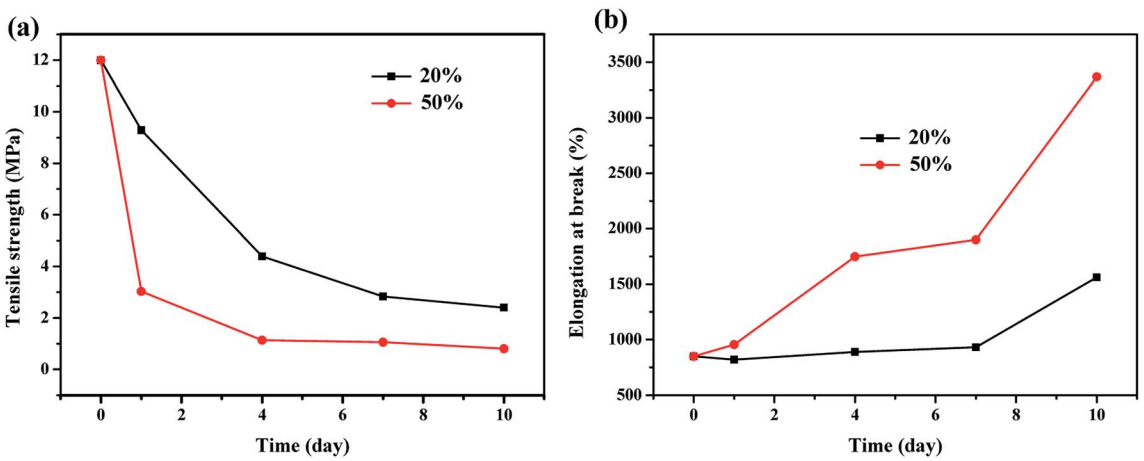

Fig. 9 (a) Tensile strength and (b) elongation at break of FKM composite immersed in HNO_3 solution for different times.

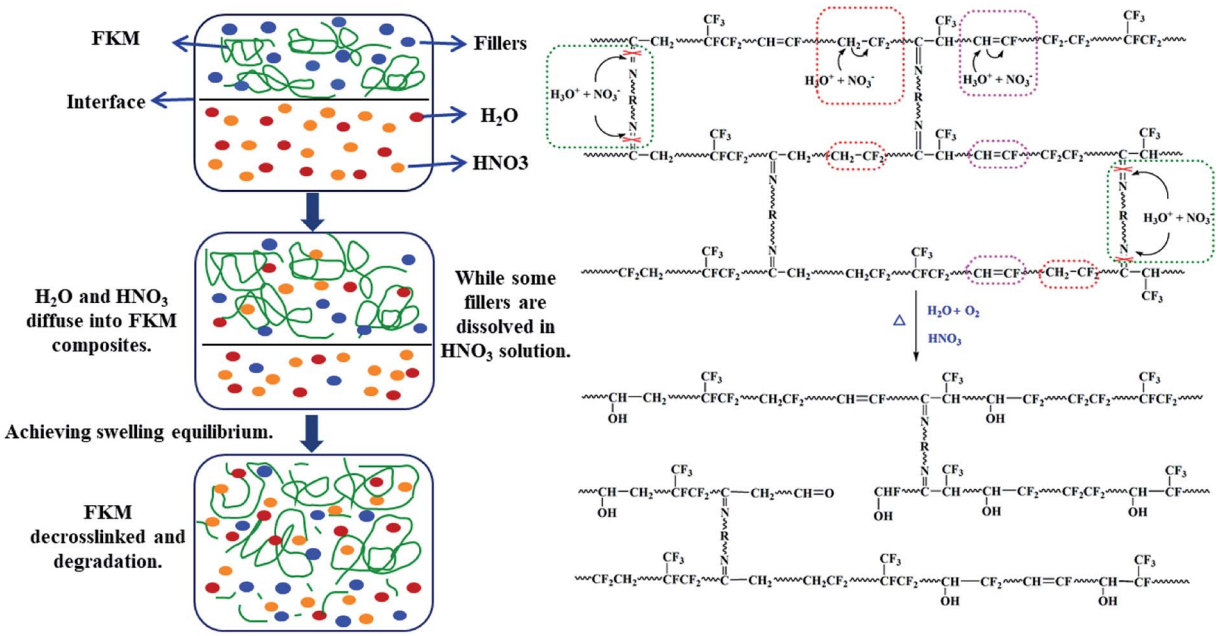

Scheme 1 Plausible diffusion and degradation mechanisms of FKM composite in HNO_3 solution.

(C═N) in an aqueous acidic environment and finally results in decrosslinking *via* hydrolysis. This is also manifested by the decrease in crosslinking degree and mechanical properties. The hydrolysis of C═N forms the oxygen-containing functional groups containing O–H, –COOH, and C═O. The presence of these oxygen-containing groups in the backbone results in the cleavage of the backbone, leading to degradation.

Moreover, the dehydrofluorination reaction of FKM proceeds through an autocatalytic reaction upon heating in an acidic environment. The increase in C═C is evident in the ATR-FTIR and MAS-NMR spectra of the FKM composite. We postulate that the electrophilic attack on C═C plausibly takes place through H_3O^+ and/or NO_3^-. This leads to the formation of a tertiary alcohol, which does not undergo further oxidation. Besides, the unsaturated bonds of the elastomer are susceptible to attack by the radicals upon heating, leading to chain scission.

4. Conclusion

The diffusion and degradation of an FKM composite induced in HNO_3 solution were studied for different immersion times and concentrations of HNO_3 solution. The weight gain and penetration distance both increased rapidly with an increase in the immersion time and concentration of the HNO_3 solution, demonstrating strong physical and chemical reactions between the FKM macromolecules and the HNO_3 solution. The diffusion process of the HNO_3 solution in FKM conformed to the classical Fick diffusion model at a low concentration of HNO_3 solution. The increase in the swelling index also manifested that the degree of degradation becomes more evident with an increase in the concentration of the HNO_3 solution. The ATR-FTIR, MAS-NMR and SEM-EDS results showed that: (i) the decrosslinking of FKM is caused by hydrolytic attack on the crosslink sites and (ii) the backbone cleavage of FKM is caused by the dehydrofluorination induced by the harsh acidic environment.

Conflicts of interest

There are no conflicts to declare.

Acknowledgements

This work was supported by the National Natural Science Foundation of China (No. 51573098), the Program for Young and Middle-aged Scientific and Technological Innovative Talents of Shenyang, China (No. RC180154), and Natural Science Foundation of Liaoning, China (No. 2019-MS-263).

References

1 S. H. Rose, Synthesis of phosphonitrilic fluoroelastomers, *J. Polym. Sci., Part B: Polym. Lett.*, 1968, **6**, 837–839.
2 R. G. Arnold, A. L. Barney and D. C. Thompson, *Rubber Chem. Technol.*, 1973, **46**, 619–652.
3 R. E. Uschold, Fluoroelastomers: Today's Technology and Tomorrow's Polymers, *Polym. J.*, 1985, **17**, 253–263.
4 B. Améduri, B. Boutevin and G. Kostov, Fluoroelastomers: synthesis, properties and applications, *Prog. Polym. Sci.*, 2001, **26**, 105–187.
5 B. Ameduri and B. Boutevin, Update on fluoroelastomers: from perfluoroelastomers to fluorosilicones and fluorophosphazenes, *J. Fluorine Chem.*, 2005, **126**, 221–229.
6 Y. Wang and Y. Bai, The functionalization of fluoroelastomers: approaches, properties, and applications, *RSC Adv.*, 2016, **6**, 53730–53748.

7 M. A. Kader and A. K. Bhowmick, Thermal ageing, degradation and swelling of acrylate rubber, fluororubber and their blends containing polyfunctional acrylates, *Polym. Degrad. Stab.*, 2003, **79**, 283–295.
8 S. Mitra, A. Ghanbari-Siahkali, P. Kingshott, S. Hvilsted and K. Almdal, Chemical degradation of an uncrosslinked pure fluororubber in an alkaline environment, *J. Polym. Sci., Part A: Polym. Chem.*, 2004, **42**, 6216–6229.
9 S. Mitra, A. Ghanbari-Siahkali, P. Kingshott, K. Almdal, H. Kem Rehmeier and A. G. Christensen, Chemical degradation of fluoroelastomer in an alkaline environment, *Polym. Degrad. Stab.*, 2004, **83**, 195–206.
10 D. Li and M. Liao, Dehydrofluorination mechanism, structure and thermal stability of pure fluoroelastomer (poly(VDF-ter-HFP-ter-TFE) terpolymer) in alkaline environment, *J. Fluorine Chem.*, 2017, **201**, 55–67.
11 Y. Wang, L. Liu, Y. Luo and D. Jia, Aging behavior and thermal degradation of fluoroelastomer reactive blends with poly-phenol hydroxy EPDM, *Polym. Degrad. Stab.*, 2009, **94**, 443–449.
12 S. Akhlaghi, A. M. Pourrahimi, C. Sjöstedt, M. Bellander, M. S. Hedenqvist and U. W. Gedde, Degradation of fluoroelastomers in rapeseed biodiesel at different oxygen concentrations, *Polym. Degrad. Stab.*, 2017, **136**, 10–19.
13 L. Xia, M. Wang, H. Wu and S. Guo, Effects of cure system and filler on chemical aging behavior of fluoroelastomer in simulated proton exchange membrane fuel cell environment, *Int. J. Hydrogen Energy*, 2016, **41**, 2887–2895.
14 H. Hori, H. Tanaka, T. Tsuge, R. Honma, S. Banerjee and B. Ameduri, Decomposition of fluoroelastomer: Poly(vinylidene fluoride-ter-hexafluoropropylene-ter-tetrafluoroethylene) terpolymer in subcritical water, *Eur. Polym. J.*, 2017, **94**, 322–331.
15 S. H. Kalfayan, R. H. Silver and S. S. Liu, Accelerated Heat-Aging Studies on Fluororubber in Various Media, *Rubber Chem. Technol.*, 1976, **49**, 1001–1009.
16 N. K. Sinha, R. Mukhopadhyay and B. Raj, Mechanical behavior of fluoroelastomer considering long term ageing, *Nucl. Eng. Des.*, 2013, **254**, 89–96.
17 T. Sugama, T. Pyatina, E. Redline, J. McElhanon and D. Blankenship, Degradation of different elastomeric polymers in simulated geothermal environments at 300 °C, *Polym. Degrad. Stab.*, 2015, **120**, 328–339.
18 D. Li and M. Liao, Study on the dehydrofluorination of vinylidene fluoride (VDF) and hexafluoropropylene (HFP) copolymer, *Polym. Degrad. Stab.*, 2018, **152**, 116–125.
19 C.-W. Lin, C.-H. Chien, J. Tan, Y. J. Chao and J. W. Van Zee, Chemical degradation of five elastomeric seal materials in a simulated and an accelerated PEM fuel cell environment, *J. Power Sources*, 2011, **196**, 1955–1966.
20 J. Tan, Y. J. Chao, J. W. Van Zee, X. Li, X. Wang and M. Yang, Assessment of mechanical properties of fluoroelastomer and EPDM in a simulated PEM fuel cell environment by microindentation test, *Mater. Sci. Eng. A*, 2008, **496**, 464–470.
21 J. Tan, Y. J. Chao, M. Yang, W.-K. Lee and J. W. Van Zee, Chemical and mechanical stability of a Silicone gasket material exposed to PEM fuel cell environment, *Int. J. Hydrogen Energy*, 2011, **36**, 1846–1852.
22 J. Tan, Y. J. Chao, H. Wang, J. Gong and J. W. Van Zee, Chemical and mechanical stability of EPDM in a PEM fuel cell environment, *Polym. Degrad. Stab.*, 2009, **94**, 2072–2078.
23 J. Dai, X. Yao, H. Y. Yeh and X. Liang, Moisture absorption of filled silicone rubber under electrolyte, *J. Appl. Polym. Sci.*, 2006, **99**, 2253–2257.
24 H. Jiang, Q. Yu, H. Li, H. Tao, L. Zhong and N. Yan, Moisture Diffusion Property and Moisture-induced Electrical Performances of Liquid Silicone Rubber *Condition Monitoring and Diagnosis (CMD)2018*, 2018, pp. 1–5.
25 Y. Gao, X. Liang, J. Wang, Z. Yan, Y. Liu and Y. Cai, A capacitance study of anomalous diffusion of water into HTV silicone rubber materials, *IEEE Trans. Dielectr. Electr. Insul.*, 2016, **23**, 368–376.
26 Y. Gao, X. Liang, W. Bao, S. Li, C. Wu and Y. Liu, *et al.*, Effects of liquids immersion and drying on the surface properties of HTV silicone rubber: characterisation by contact angle and surface physical morphology. *High Voltage*, Institution of Engineering and Technology, 2019, pp. 49–58.
27 Z. Wang, Z. D. Jia, M. H. Fang and Z. C. Guan, Absorption and permeation of water and aqueous solutions of high-temperature vulcanized silicone rubber, *IEEE Trans. Dielectr. Electr. Insul.*, 2015, **22**, 3357–3365.
28 J. F. Narváez Valderrama, K. Baek, F. J. Molina and I. J. Allan, Implications of observed PBDE diffusion coefficients in low density polyethylene and silicone rubber, *Environ. Sci.: Processes Impacts*, 2016, **18**, 87–94.
29 J. Crank, *The mathematics of diffusion*, Oxford, Oxford university, 1979.
30 G. Unnikrishnan, S. Thomas and S. Varghese, Sorption and diffusion of aromatic hydrocarbons through filled natural rubber, *Polymer*, 1996, **37**, 2687–2693.
31 I. McEwan, R. A. Pethrick and S. J. Shaw, Water absorption in a rubber-modified epoxy resin; carboxy terminated butadiene acrylonitrile-amine cured epoxy resin system, *Polymer*, 1999, **40**, 4213–4222.
32 S. Mitra, A. Ghanbari-Siahkali, P. Kingshott, H. K. Rehmeier, H. Abildgaard and K. Almdal, Chemical degradation of crosslinked ethylene-propylene-diene rubber in an acidic environment. Part II. Effect of peroxide crosslinking in the presence of a coagent, *Polym. Degrad. Stab.*, 2006, **91**, 81–93.
33 S. Mitra, A. Ghanbari-Siahkali, P. Kingshott, H. K. Rehmeier, H. Abildgaard and K. Almdal, Chemical degradation of crosslinked ethylene-propylene-diene rubber in an acidic environment. Part I. Effect on accelerated sulphur crosslinks, *Polym. Degrad. Stab.*, 2006, **91**, 69–80.